J. Membrane Biol. 156, 261–277 (1997)

The Journal of
Membrane
Biology

Characterization of Angiotensin II-regulated K^+ Conductance in Rat Adrenal Glomerulosa Cells

D.P. Lotshaw
Department of Biological Sciences, Northern Illinois University, DeKalb, IL 60115, USA

Received: 6 August 1996/Revised: 15 November 1996

Abstract. Nystatin perforated-patch clamp and single-channel recording methods were used to characterize macroscopic and single-channel K^+ currents and the effects of angiotensin II (AngII) in cultured rat adrenal glomerulosa cells. Two basic patterns of macroscopic current-voltage relationships were observed: type 1 exhibited a rapidly activating, noninactivating, voltage-dependent outward current and type 2 exhibited an inactivating voltage-dependent outward current attributed to charybdotoxin sensitive Ca^{++}-dependent K^+ channels. Most cells exhibited the type 1 pattern and experiments focused on this cell type. Cell-attached and inside-out patches were dominated by a single K^+ channel class which exhibited an outward conductance of 12 pS (20 mM K^+ pipette in cell-attached and inside-out configurations, 145 mM K^+_{in}), a mean open time of 2 msec, and a weakly voltage-dependent low open probability that increased with depolarization. Channel open probability was reversibly inhibited by bath stimulation with AngII. At the macroscopic level, type 1 cell macroscopic K^+ currents appeared comprised of two components: a weakly voltage-dependent current controlling the resting membrane potential (−85 mV) which appeared mediated by the 12 pS K^+ channel and a rapidly activating, noninactivating voltage-dependent current activated above −50 mV. The presence of the second voltage-dependent K^+ channel class was suggested by the effects of AngII, the blocking effects of quinidine and Cs^+, and the properties of the weakly voltage-dependent K^+ channel described. The K^+ selectivity of the macroscopic current was demonstrated by the dependence of current reversal potentials on the K^+ equilibrium potential and by the effects of K^+ channel blockers, Cs^+ and quinidine. AngII (10 pM to 1 nM) reversibly inhibited macroscopic K^+ currents and this effect was blocked by the AT_1 receptor antagonist losartin.

Key words: Aldosterone — Angiotensin II — Angiotensin II type 1 receptor — Losartin — Potassium channels — Quinidine

Introduction

The K^+ channel classes controlling the plasma membrane potential and, consequently, Ca^{++} influx through voltage-dependent Ca^{++} channels have been hypothesized to play an important role in mediating regulation of aldosterone secretion from adrenal glomerulosa cells [*for review see* 2, 21]. The resting membrane ionic conductance of these cells is dominated by K^+ [12, 18] and angiotensin II (AngII)-induced membrane depolarization has been attributed to inhibition of K^+ channels [3, 15, 17, 19]. However, there is little agreement among different laboratories regarding the properties of the K^+ channels controlling the membrane potential even within the same species. Whole-cell patch-clamp measurements of macroscopic K^+ currents described two basic patterns of depolarization-activated K^+ current inhibited by AngII or adrenocorticotropic hormone (ACTH) in rat, bovine and human glomerulosa cells. One pattern may be described as exhibiting a delayed rectifier-type of rapidly-activating, noninactivating current; the second pattern exhibited pronounced inactivation of the outward current [3, 15, 16, 17]. Brauneis et al. [3] reported that the noninactivating delayed rectifier pattern predominated in rat cells and was also observed in some human cells whereas the transient pattern of outward current was predominant in bovine cells and also observed in human cells. Payet et al. [17] reported that human cells exhibited the transient current pattern and that this current was blocked by 2 mM 4-aminopyridine, suggesting an A-type K^+ current. In contrast to the results of Brau-

Correspondence to: D.P. Lotshaw

neis et al. [3], Payet et al. [16] reported that a transient outward current pattern predominated in rat cells and attributed the current to Ca^{++}-dependent maxi-K^+ channels. None of these studies characterized the macroscopic K^+ current controlling the resting membrane potential although it was suggested that Ca^{++}-dependent maxi-K^+ channels control the resting membrane potential in rat cells [16]. At the single-channel level the predominant channel observed in cell-attached patches from both rat and bovine cells was reported to be an inwardly rectifying K^+ channel inhibited by bath application of AngII [10, 24]. These authors also reported AngII inhibition of a second class of noninactivating K^+ permeable channels postulated to mediate delayed rectification in rat cells.

The discrepancies between these studies have not been resolved and may reflect differences in cell culture conditions or electrophysiological methods. At the single-channel level the properties of the AngII-modulated, inwardly-rectifying K^+ channel were not reconciled with the lack of inward rectification in the macroscopic currents measured under whole-cell patch clamp. This might suggest that some AngII-modulated K^+ channels rapidly rundown under whole–cell recording conditions.

The purpose of the present study was to characterize macroscopic and single-channel K^+ currents and to examine AngII effects on K^+ currents in rat adrenal glomerulosa cells. To reduce channel rundown or loss of normal signal transduction processes, the nystatin perforated-patch technique [8] was substituted for whole-cell patch clamp. This method restricts exchange between the pipette solution and cytosol to solutes permeable to the nystatin-formed pore, primarily small monovalent ions [5].

Materials and Methods

Cell Culture

Primary cultures of rat adrenal zona glomerulosa cells were prepared by collagenase digestion of the capsular portion of the adrenal glands from female Sprague-Dawley rats weighing between 125–175 gm (Harlan, Indianapolis, IN) as described [9]. Briefly, animals were anesthetized by ether inhalation prior to euthanasia by decapitation. Adrenal glands were removed and placed in an ice-cold, modified Hanks' saline (*composition below*). Glands were dissected free of adherent fat and the capsular portion containing the zona glomerulosa layer was removed and cut into small pieces. The capsular fragments were washed twice with the saline containing 0.2% fatty acid free bovine serum albumin (BSA) followed by incubation for 1 hr at 37°C in oxygenated saline containing 0.2% BSA, 1.0 mg/ml collagenase, and 25 μg/ml deoxyribonuclease I. Incubation was stopped with ice-cold saline and the tissue was washed four times by repeated cycles of centrifugation and resuspension in fresh 0.2% BSA saline to remove enzymes and cellular debris. The tissue was triturated through a small bore pipette to separate cells and the resulting cell suspension was filtered through a 70 μm pore size nylon screen. Cells were pelleted by centrifugation, resuspended in culture medium and plated at low density (less than 10^5 cells/ml) on fibronectin treated glass coverslip chips. Cultures were maintained at 37°C in an humidified atmosphere of 5% CO_2–95% air. Culture medium consisted of a mixture of Ham's F-12 and Dulbecco's modified Eagle's medium (1:1) supplemented with 2% fetal calf serum, 8% horse serum, 0.1 mM ascorbic acid, 1 μM vitamin E, 1 μg/ml insulin, 50 U/ml penicillin G, and 50 μg/ml streptomycin.

Sera were obtained from GIBCO-BRL, Grand Island, NY and collagenase from Worthington, Freehold, NJ; all other reagents were obtained from Sigma (St. Louis, MO). Losartan (DuP753) was a generous gift from Du Pont (Wilmington, DE). Aldosterone was measured without extraction by radioimmunoassay (Diagnostic Products, Los Angeles, CA).

Electrophysiology

Patch-clamp recordings [7, 8] were performed on cells maintained in culture from 2 to 72 hr. However, formation of the gigaohm seal between the pipette and plasma membrane was often difficult in freshly isolated cells, possibly due to insufficient digestion of cell surface macromolecules during tissue dissociation. Gigaohm seals were readily obtained on cells maintained in culture overnight (or at least 12 hr). Glass coverslip chips containing adherent glomerulosa cells were transferred to a small volume (0.5 ml) recording chamber mounted on an inverted microscope equipped with phase contrast optics. The chamber was continuously perfused at a rate of 1 ml/min with modified Hanks' saline equilibrated with 100% O_2 (in mM): 140 NaCl, 4 KCl, 1.25 $CaCl_2$, 1.2 $MgCl_2$, 4.2 $NaHCO_3$, 10 N-2-hydroxyethylpiperazine-N′-2-ethanesulfonic acid (HEPES), 5.5 glucose, pH adjusted to 7.4 with NaOH. For experiments in which the KCl concentration of the saline was increased, the NaCl concentration was reduced by an equimolar amount. Sodium methanesulfonate was used in low Cl^- saline, replacing an equimolar amount of NaCl. In some experiments a high K^+ saline was used to zero the resting membrane potential (in mM): 145 KCl, 2.5 $MgCl_2$, 5 glucose, 10 HEPES, pH adjusted to 7.4 with KOH. All recordings were performed at room temperature.

The perforated-patch variation of the whole-cell patch clamp was employed using nystatin as the pore forming agent [8]. A stock solution of nystatin dissolved in dimethylsulfoxide (50 mg/ml) was freshly prepared each day and diluted in pipette solution to a concentration of 200 μg/ml. The patch pipette solution contained (in mM): 55 KCl, 70 K_2SO_4, 8 $MgCl_2$, 10 HEPES, pH adjusted to 7.3 with KOH. In some experiments Cs^+ was substituted for K^+ in the nystatin-pipette solution (in mM): 55 CsCl, 70 Cs_2SO_4, 8 $MgCl_2$, 10 HEPES, pH adjusted to 7.3 with CsOH. Patch pipettes were fabricated from Corning 7052 capillary glass to give a pipette resistance of 3 to 4 megohms when filled with pipette solution as described. Pipettes were coated with sylgard (Dow Corning, Midland, MI) to within 100 μM of the tip. Membrane potentials were corrected for liquid junction potentials as described [14].

Pipettes for cell-attached and inside-out patch clamp were constructed using borosilicate TW-150 glass capillaries (World Precision Instruments, Sarasota, FL) to give pipette resistances of 6 to 8 megohms when filled with pipette saline as described above. The KCl and NaCl concentrations of the pipette solutions were varied but the sum of their concentrations was always 145 mM, in general the pipette solution contained (in mM): 145 KCl + NaCl, 2 $MgCl_2$, 0.1 $CaCl_2$, 10 HEPES, pH adjusted to 7.4 with NaOH.

Membrane current was measured with a Axopatch 200 amplifier (Axon Instruments, Foster City, CA). Macroscopic currents were low pass filtered at 10 kHz (−3 dB) with a four-pole Bessel filter. Currents were sampled at 10 KHz or 20 KHz (TL-1-125 analog-to-digital con-

verter, Axon Instruments) and stored on computer for subsequent analysis with PCLAMP software (Axon Instruments). Single-channel currents were low-pass filtered at 2 KHz and stored on computer or using a digital audiotape recorder (Sony, Japan) for subsequent analysis. For computer analysis of recorded data, current records were sampled at 10 KHz during playback; events were selected for analysis by the 50% of current amplitude threshold criteria and analyzed for mean current amplitude and open times with PCLAMP software. Mean channel open times were determined from single exponential fits to open time histograms. Single-channel open probability was determined from 10-sec episodes of continuous recording and calculated as:

$$NP_o \stackrel{N}{=} \sum_{n=1} nt_n, \quad (1)$$

where P_o represents the single-channel open probability, t_n represented the fraction of the analysis period with n open channels and N represents the maximum number of simultaneously open channels in the record. In the figures of single-channel current recordings, downward current deflections represented inward current.

Results

Glomerulosa cells were identified by visual appearance under phase contrast microscopy. In culture, adherent cells identified as glomerulosa cells initially retained their characteristic spherical shape and granular cytoplasm. Over one-to-two days in culture, many cells flattened and extended short processes along the substrate as described [20]. After two days in culture, cells retained their ability to secrete aldosterone in response to hormone stimulation; one hr stimulation with 1 nM AngII or 100 pM ACTH increased aldosterone fivefold and thirty-fivefold over basal secretion, respectively.

Patterns of Macroscopic Membrane Current

Two patterns of macroscopic current-voltage (*IV*) relationships were observed in the cultured cells using the nystatin perforated-patch clamp. One pattern, referred to as type 1, consisted of a rapidly activating, noninactivating outward current response to depolarizing voltage commands from a holding potential of −90 mV and no inwardly rectifying current in response to membrane hyperpolarization (Fig. 1). In other experiments, outward current was maintained for pulse durations of up to 0.5 sec indicating that the current did not exhibit slow inactivation (*data not shown*). However, some cells exhibited a small transient component (*see* Fig. 6). The holding potential, −90 mV, was near the average resting membrane potential of these cells, −87.2 ± 6.4 mV (mean ± SD) measured as the zero membrane current potential). Transient inward currents evoked by depolarizing voltage commands above −50 mV were also observed however in most cells inward currents were small and usually obscured by outward current.

The second *IV* pattern, referred to as type 2, consisted of a transient outward current activated by depolarizing voltage commands from a holding potential of −90 mV and often, but not always, exhibited a small inwardly rectifying current response to hyperpolarizing voltage commands (Fig. 2). As in the type 1 pattern, depolarization-activated inward currents were small and obscured by outward currents. Bath stimulation of the type 2 cells with 1 nM AngII inhibited the peak depolarization-activated outward current and increased its rate of inactivation (Fig. 2*A*); reversal of AngII inhibition of membrane current was rarely observed under this recording condition. The depolarization-activated outward current was predominantly attributable to the Ca^{++}-dependent maxi-K^+ channel. This was demonstrated by the sensitivity of the outward current to block by 50 nM charybdotoxin (Fig. 2*C*) and low concentrations (5 mM) of extracellular tetraethylammonium chloride (TEA) (*data not shown*). Furthermore, single maxi-K^+ channel currents were readily observed in single-channel studies particularly in the older cultures (*data not shown*). Cells exhibiting the type 1 *IV* pattern were largely unaffected by charybdotoxin suggesting that these cells did not express a significant number of Ca^{++}-dependent maxi-K^+ channels.

The remainder of the results will address the properties of cells expressing the type 1 *IV* relationship. This *IV* relationship may represent the predominant phenotype of glomerulosa cells *in vivo;* this relationship was observed in all acutely dissociated cells examined (n = 10) and in most of the cells maintained in culture for less than 24 hr (>80%). The type 2 *IV* pattern was observed more commonly in cells maintained for greater than 24 hr in culture suggesting that culture conditions either induced this phenotype or selected for the survival of this cell type. Gradations between the type 1 and type 2 *IV* relationships were occasionally observed. We have been unable to predict which *IV* pattern will be observed prior to recording based on cell morphology.

Type 1 AngII-modulated Macroscopic K^+ Current

The steady-state *IV* relationship of the type 1 cell may be divided into two main components: (i) a weakly voltage-dependent ''leak'' current active at the resting membrane potential and (ii) the rapidly activating, noninactivating outward current analogous to delayed rectifier K^+ currents found in many cell types. Stimulation by bath perfusion of AngII reversibly inhibited both the weakly voltage-dependent leak current and the depolarization-activated outward current (Fig. 1). Inhibition of both components of membrane current was observed at AngII concentrations as low as 10 pM and no differences between the sensitivity of either component was detected. A stable level of current inhibition required approximately 10-min exposure at bath concentrations below 0.1

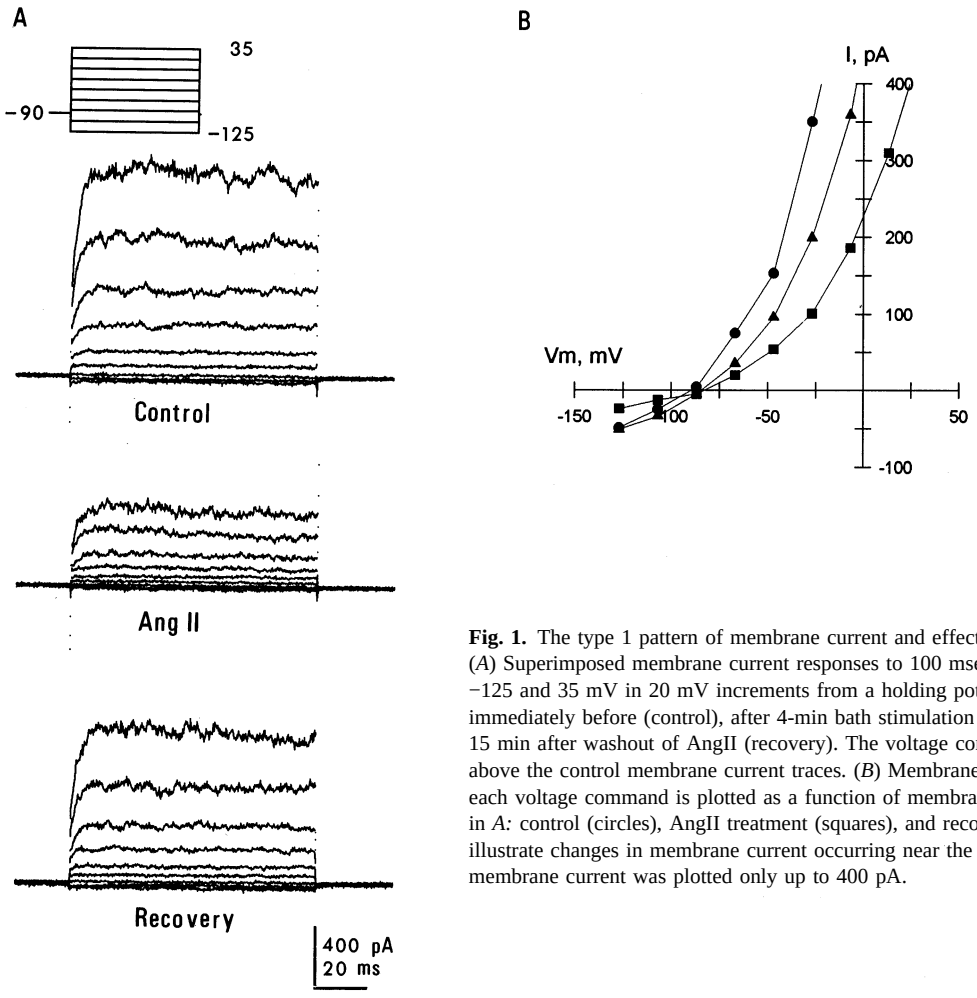

Fig. 1. The type 1 pattern of membrane current and effect of AngII on the *IV* relationship. (*A*) Superimposed membrane current responses to 100 msec voltage commands between −125 and 35 mV in 20 mV increments from a holding potential of −90 mV are shown immediately before (control), after 4-min bath stimulation with 1.0 nM AngII (Ang II), and 15 min after washout of AngII (recovery). The voltage command paradigm is illustrated above the control membrane current traces. (*B*) Membrane current measured at the end of each voltage command is plotted as a function of membrane potential from records shown in *A:* control (circles), AngII treatment (squares), and recovery (triangles). To clearly illustrate changes in membrane current occurring near the holding potential, outward membrane current was plotted only up to 400 pA.

nM AngII and at least 5 min at higher concentrations. AngII-induced inhibition appeared to saturate when cells were exposed to 1 nM AngII for several minutes. Recovery from AngII-induced inhibition was usually maximal within 15 to 20 min after AngII washout; the depolarization-activated outward current usually recovered more rapidly than the weakly voltage-dependent component.

The effect of AngII on the steady state *IV* relationship (Fig. 1*B*) was plotted to illustrate modulation of the weakly voltage-dependent leak current. Measured as the change in slope conductance, 0.5 to 1.0 nM AngII decreased the linear slope conductance to 47% of the control (average, range was between 20% to 80% inhibition, $n = 16$) measured between −85 and −125 mV. The reversal potential of the AngII-modulated current was −88.9 ± 4.5 mV (mean ± SD, $n = 16$), measured as the intersection of the *IV* curves for the control and AngII stimulated steady-state current (Fig. 1*B*). The reversal potential of the AngII-modulated current was close to the expected equilibrium potential for K^+ suggesting modulation of a K^+ current. The K^+ selectivity of this current was demonstrated by examining the effects of elevated extracellular K^+ concentration on the reversal potential of the AngII-modulated component of leak current (Fig. 3). Increasing extracellular K^+ increased the slope conductance of the *IV* curve and shifted the curve to the right as expected for a K^+ selective conductance (Fig. 3*B*). In 10 mM K^+ small inward current relaxations were induced by the most negative voltage commands (to −125 mV) (Fig. 3*A*). This current relaxation represented deactivation of the leak K^+ current which was visible in 10 mM K^+ and not 4 mM K^+ due to the increased K^+ conductance. Increased K^+ conductance was due to the increased extracellular K^+ concentration as well as the more depolarized holding potential (−65 mV) used to avoid maintaining a large holding current in 10 mM K^+. The reversal potential of the AngII-modulated current also shifted to the right with elevation of extracellular K^+ as expected for modulation of K^+-selective conductance (Fig. 3*C*). The slope of the regression line was 45 mV/10-fold change in extracellular K^+ concentration. This value is somewhat less than expected for modulation of

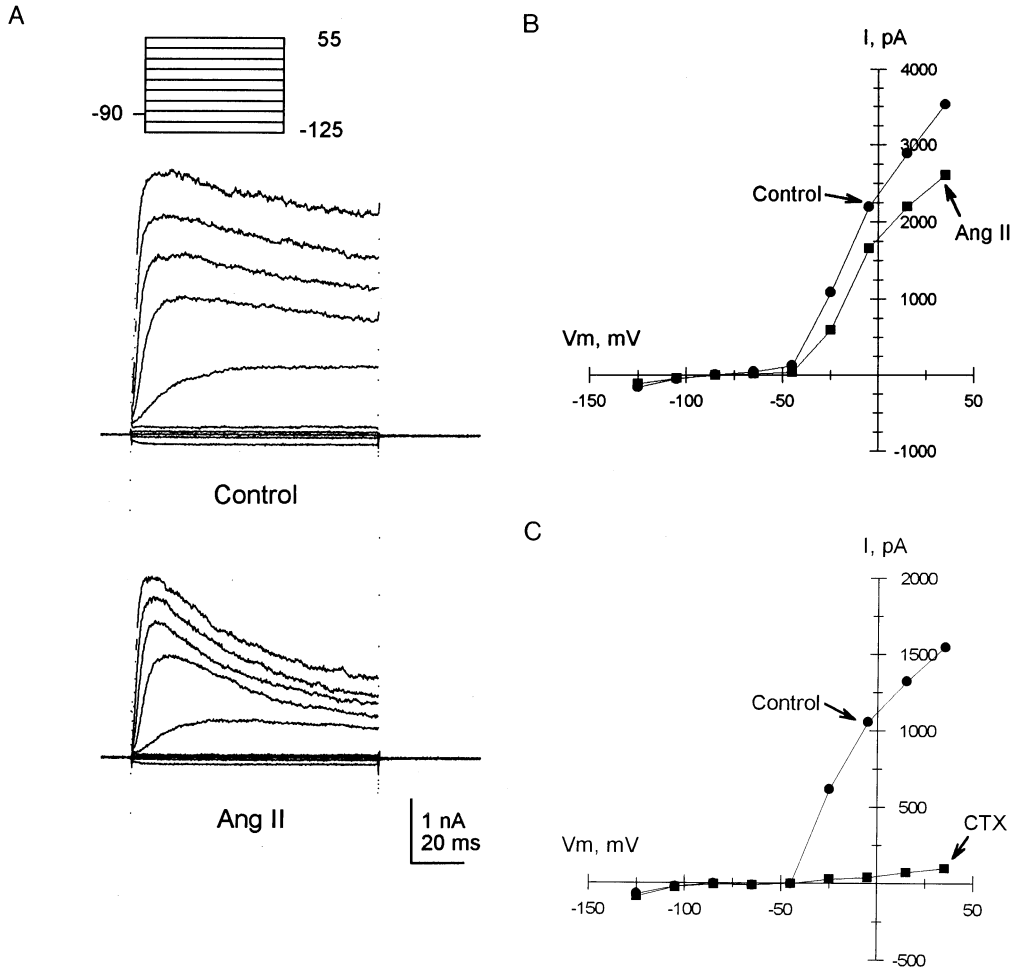

Fig. 2. The type 2 pattern of membrane current and effect of AngII and charybdotoxin on the *IV* relationship. (*A*) Superimposed membrane current responses to 100 msec voltage commands between −125 and 55 mV in 20 mV increments from a holding potential of −90 mV are shown immediately before (control), after 4-min bath stimulation with 1.0 nM AngII (Ang II). The voltage command paradigm is illustrated above the control membrane current traces. (*B*) Peak current measured during each voltage command is plotted as a function of membrane potential from records shown in *A:* control (circles), AngII treatment (squares). (*C*) Effect of 50 nM charybdotoxin on peak membrane current-voltage relationship measured as in (*A*) in another type 2 cell: control (circles), charybdotoxin (squares).

a perfectly K^+ selective conductance (approximately 58 mV/10-fold change in K^+ concentration).

Cl^- currents did not contribute significantly to the steady-state leak current. Reducing extracellular Cl^- concentration by substituting sodium methanesulfonate for 50% of the extracellular NaCl in the bath saline did not alter the control *IV* relationship or the reversal potential of the AngII-modulated component of membrane current (*data not shown*). The current reversal potential induced by 1 nM AngII was −92.5 ± 2.5 mV (mean ± SD, $n = 3$) in the low Cl^-, 4 mM K^+ saline and −87.2 ± 6.4 mV (mean ± SD, $n = 9$) in normal extracellular Cl^-, 4 mM K^+. If AngII also modulated a Cl^- conductance then the reversal potential would have been expected to shift to a more depolarized membrane potential, assuming methanesulfonate was impermeable relative to Cl^-.

Type 1 Depolarization-activated K^+ Current

As shown in Fig. 1, AngII reduced a depolarization-activated, noninactivating outward current. Tail currents were utilized to examine ion selectivity, voltage-dependence and AngII modulation of outward current (Fig. 4). Tail current amplitudes were directly proportional to the amplitude of the outward current, indicating that tail currents represented deactivation of depolarization-activated outward current (*data not shown*). Tail current relaxations were well fit by single exponential functions at test potentials more negative than −45 mV suggesting that the current was predominantly comprised of a single-channel class. The tail current relaxation time constant was weakly voltage-dependent, increasing from approximately 2 msec at a test potential of −105 mV to

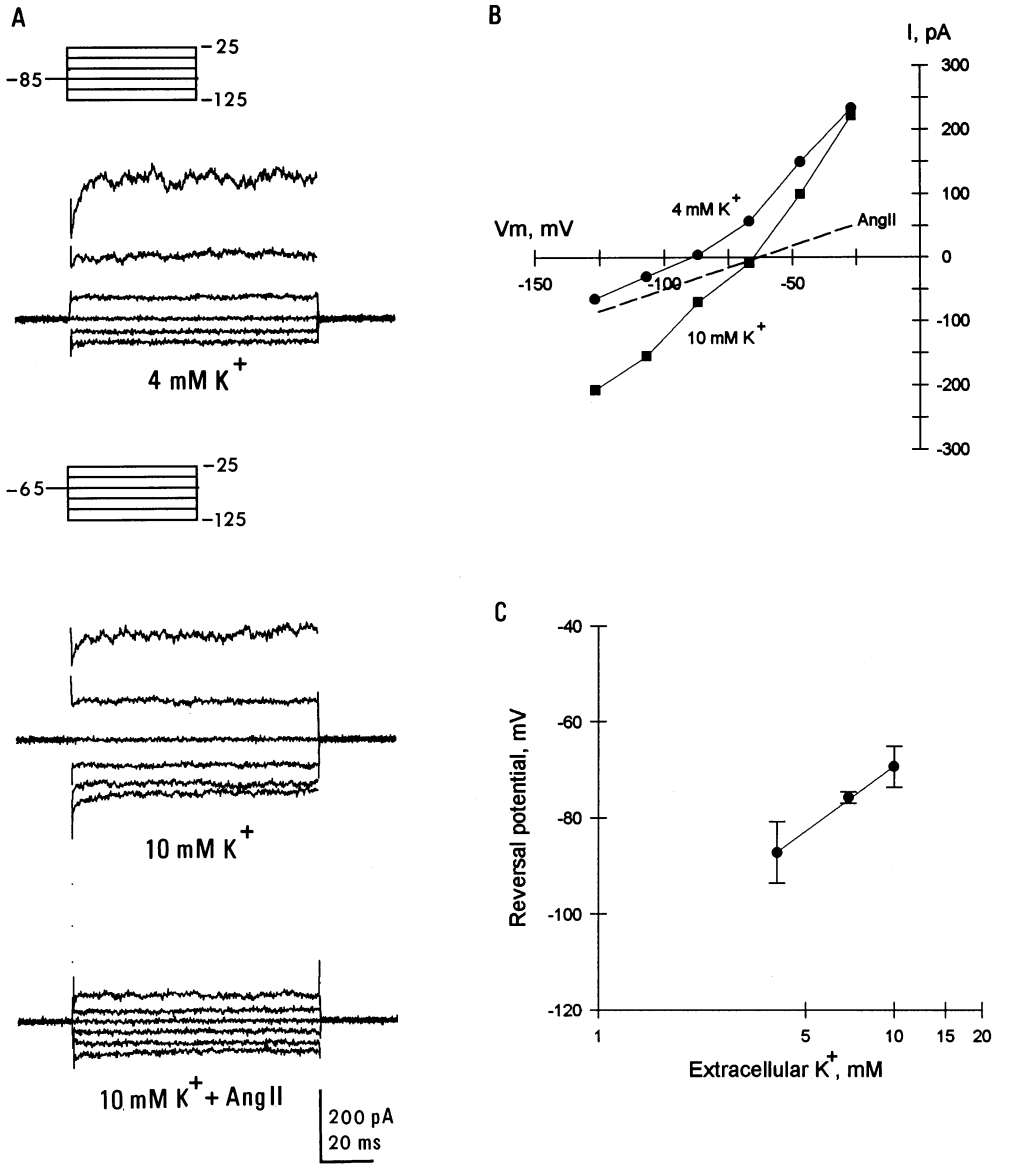

Fig. 3. Effect of elevated extracellular K^+ and AngII on the weakly voltage-dependent leak current and the reversal potential of the AngII-modulated current. (*A*) Superimposed membrane current responses to 100 msec voltage commands between −125 and −25 mV in 4 mM extracellular K^+ (uppermost traces), in 10 mM extracellular K^+ (middle traces), and during stimulation with 1 nM AngII in 10 mM K^+ (lower traces). The voltage command paradigm is illustrated above the upper and middle sets of current traces, evoked from a holding potential of −85 mV in 4 mM K^+ and −65 mV in 10 mM K^+. (*B*) *IV* plot of the instantaneous membrane current at each voltage from current traces shown in *A* for 4 mM (circles) and 10 mM (squares) extracellular K^+. The dashed line represents the membrane current values during AngII treatment. (*C*) Effect of the extracellular K^+ concentration on the reversal potential of AngII-modulated membrane current, measured as the intersection of control and AngII *IV* curves. Symbols indicate the mean ± SD of the reversal potential ($n = 9$, 3 and 6 at 4, 7 and 10 mM extracellular K^+, respectively). The line represents the least squares linear regression fit to the data.

approximately 3 msec at −45 mV. Tail current amplitude did not saturate in response to increasing pulse potentials when measured at a constant test potential (Fig. 4*D*) even with depolarizing pulses to 100 mV (*data not shown*). Control experiments indicated that tail current relaxations were not substantially affected by Ca^{++} current deactivation under the ionic conditions employed. Reducing Ca^{++} current, either by lowering extracellular Ca^{++} from 1.25 to 0.1 mM or addition of 100 μM Ni^{++} to block T-type Ca^{++} current [13], shifted the tail current reversal potential between −3 and −5 mV and slightly decreased the time constant of the relaxations at the most

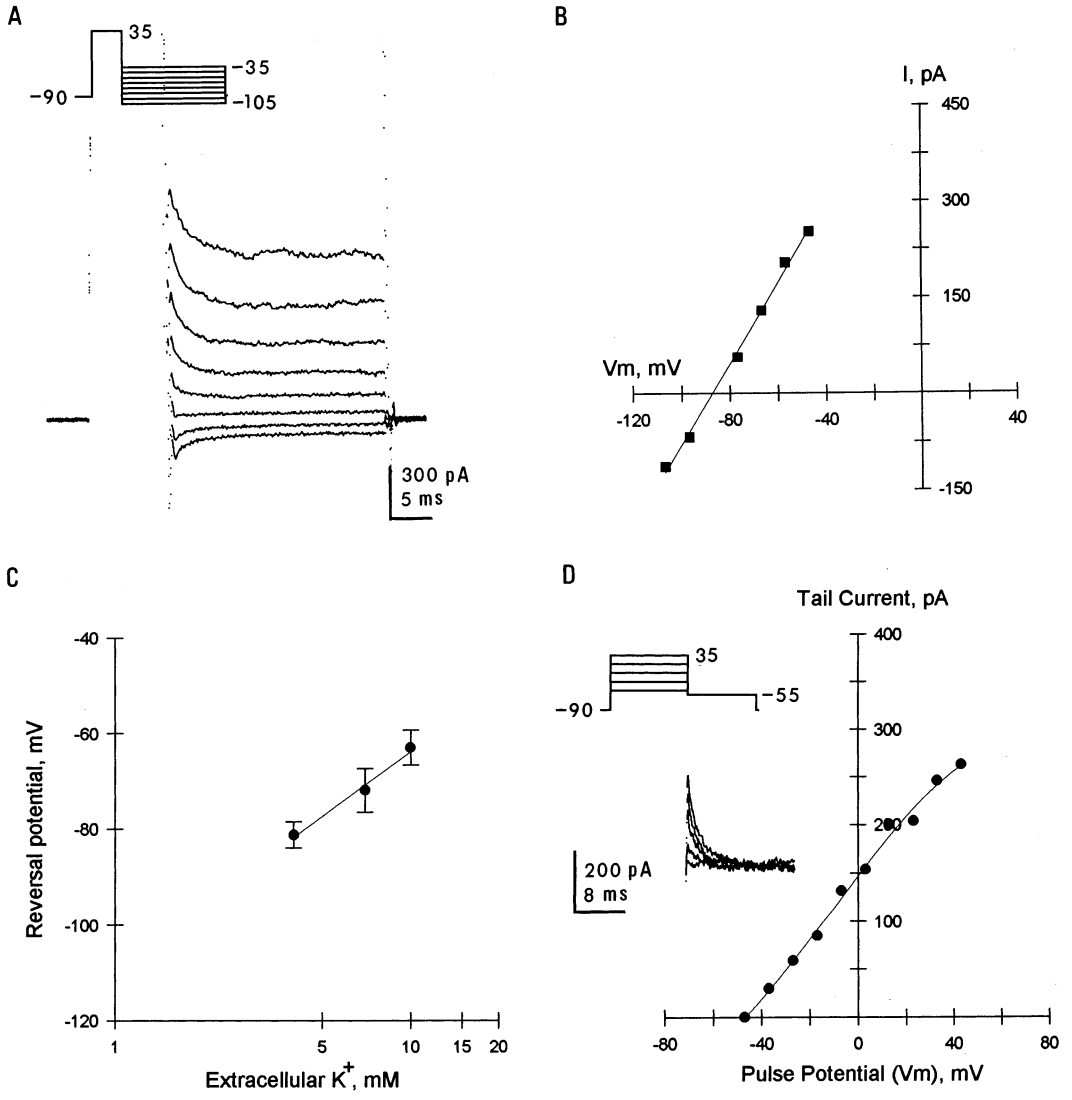

Fig. 4. Tail current analysis of the depolarization-activated outward membrane current. (*A*) Tail currents evoked by repolarization from the pulse potential (35 mV) to test potentials between −105 and −35 mV in 10 mV increments. The voltage paradigm is illustrated above the current traces. Current during the pulse potential was offscale. (*B*) Tail current amplitude plotted as a function of the test potential; amplitudes were determined from single exponential fits to the current relaxation. The reversal potential was measured as the intersection of a least squares regression fit of the data (solid line) with the voltage axis, −88 mV for this cell. (*C*) Effect of extracellular K^+ concentration on the tail current reversal potential. Symbols represent the mean ± SD of the reversal potential at each extracellular K^+ concentration (n = 10, 3 and 5 at 4, 7 and 10 mM K^+, respectively). The regression fit of the data (solid line) exhibited a slope of 45.0 mV/10 fold change in K^+. (*D*) Voltage-dependence of depolarization-activated current. The tail current evoked by increasing pulse potentials was measured at a constant test potential of −55 mV in 4 mM extracellular K^+. Pulse potentials were varied from −45 to 45 mV in 10 mV increments. The line represents a third order regression fit to the data. *Inset:* the voltage protocol employed and the tail currents evoked by pulse potentials from −45 to 35 mV; for clarity tail currents are shown for 20 mV increments in pulse potential.

hyperpolarized test potentials (*data not shown*). These treatments did not otherwise affect either outward current activation during the depolarizing command or tail current relaxations.

The tail current reversal potential was used to examine the K^+ selectivity of the depolarization-activated outward current (Fig. 4*B*). The reversal potential shifted with changes in extracellular K^+ concentration as expected for a K^+ selective current (Fig. 4*C*); the slope of the regression line was 45 mV/10-fold change in extracellular K^+ concentration. AngII decreased the tail current amplitude without affecting its reversal potential, relaxation time constants or voltage-dependence. AngII (1 nM) inhibited the tail current amplitude an average of 56% (N = 5). The effects of AngII are shown for separate experiments using 4 mM and 10 mM extracellular K^+

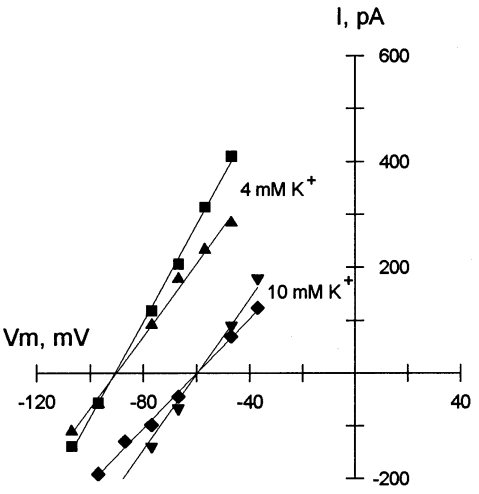

Fig. 5. The effect of 0.1 nM AngII on tail current amplitude and reversal potential measured in 4 and 10 mM extracellular K^+. Tail currents were measured as described in Fig. 4; in 4 mM extracellular K^+, control (squares) and AngII (triangles) tail current amplitudes and in 10 mM extracellular K^+, control (inverted triangles) and AngII (diamonds) tail current amplitudes. Lines represent linear regression fits to the data.

(Fig. 5). A lower AngII concentration (0.1 nM) was employed so that tail currents remained large enough to accurately reveal the reversal potential. AngII-induced tail current inhibition was not associated with a shift in reversal potential in either 4 or 10 mM K^+.

As described for leak K^+ conductance, Cl^- channels did not contribute significantly to the depolarization-activated outward current. Reducing extracellular Cl^- concentration of the bath saline by substituting sodium methanesulfonate for 50% of NaCl did not alter the depolarization-activated outward current, tail currents, tail current reversal potentials, or AngII modulation of the tail current (*data not shown*).

Effects of K^+ Channel Blockers on Type 1 Cells

The effects of several K^+ channel blockers were examined to further verify the ionic basis of the macroscopic currents and attempt to separate different K^+ current components. Application of the nonselective K^+ channel blocker Cs^+ to the cytoplasm strongly inhibited steady state membrane current at all potentials indicating that the membrane conductance is dominated by K^+ channels. Cells were Cs^+-loaded by substituting Cs^+ for K^+ in the nystatin perforated-patch pipette solution (*see* Materials and Methods). Cs^+-loading linearized the slope conductance of the steady state *IV* curve (as described in Fig. 1) to 0.020 ± 0.005 nS/pF (mean ± SD, $n = 3$) between −125 and −65 mV, increasing slightly to 0.072 ± 0.02 nS/pF between 15 to 55 mV. By comparison, the slope conductance in control cells was 0.261 ± 0.23 nS/pF (mean ± SD, $n = 12$) between −125 and −65 mV and 3.67 ± 4.38 nS/pF between 15 to 55 mV. Treatment of Cs^+-loaded cells with 1 nM AngII induced only minor changes in membrane current.

Other K^+ channel blockers examined included extracellular tetraethylammonium (TEA) which weakly inhibited both the leak K^+ current and the depolarization-activated K^+ current by approximately 30% at a concentration of 30 mM. TEA did not alter the time constant or the reversal potential of the tail currents. Neither 50 nM charybdotoxin, 5 mM 4-aminopyridine nor 10 mM 2, 3 diaminopyridine significantly inhibited macroscopic membrane currents when applied to the bath (*data not shown*).

The antiarrhythmic drug quinidine reversibly induced a voltage-dependent inhibition of membrane current at membrane potentials below −60 mV (Fig. 6). Quinidine appeared to preferentially inhibit a depolarization-activated component of K^+ current, however quinidine effects were complicated by the voltage-dependence of quinidine blocking and unblocking reactions. Extracellular quinidine caused a dose-dependent inhibition of the steady-state depolarization-activated outward current and slowed activation and deactivation kinetics. Effects on depolarization-activated current were apparent at a concentration of 10 μM quinidine; analysis of the concentration dependence of quinidine block of tail current relaxations at a membrane potential of −55 mV (Fig. 7) was fit to the Hill equation:

$$I = (1 + (K_D/[Q])^{-n})^{-1}, \quad (2)$$

where I is the normalized current, K_D is the apparent dissociation constant, $[Q]$ is quinidine concentration, and n is the Hill coefficient. This fit yielded an apparent K_D of 38 μM/L and a Hill coefficient of 1.7. These experiments were performed in 0.1 mM Ca^{++} saline to minimize Ca^{++} current deactivation effects on tail currents.

Quinidine also reduced the instantaneous current response to depolarizing voltage-clamp pulses (Fig. 6*A*) as well as the steady-state current level during tail current measurement (Fig. 6*B*), corresponding to weak inhibition of leak K^+ current. Stimulation with 1 nM AngII in the presence of 100 μM quinidine (which inhibited tail currents by greater than 80%) caused a further large reduction of remaining membrane current at depolarized membrane potentials (*data not shown*). This result would suggest that unblocked current represented a distinct class of AngII-regulated K^+ channels, the weakly voltage-dependent leak channel.

Losartin Block of AngII-induced K^+ Current Modulation

AngII-induced stimulation of aldosterone secretion was reported to be blocked by the specific AngII type 1 (AT_1)

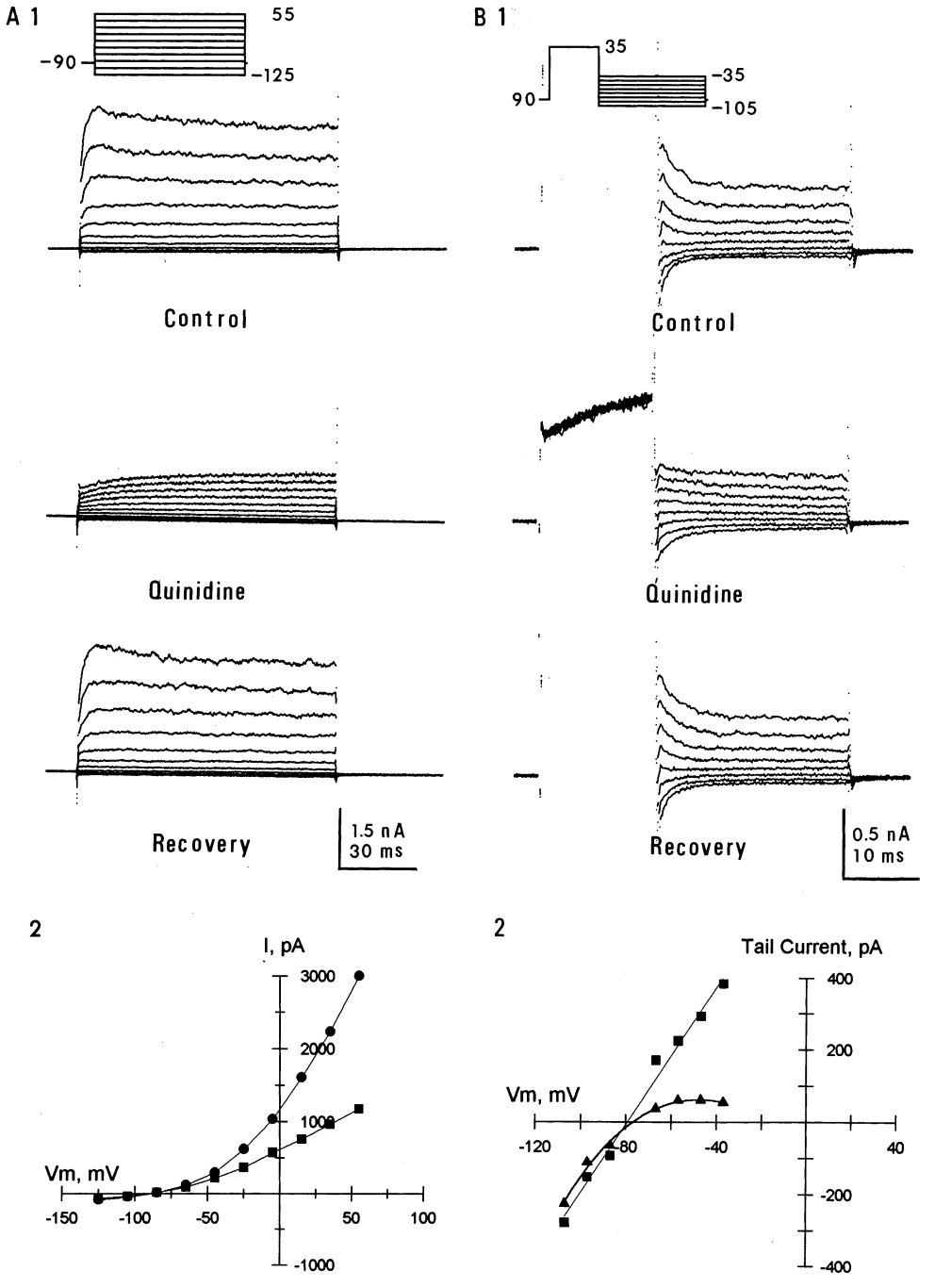

Fig. 6. Effect of quinidine on membrane currents. (*A*1) Membrane current evoked by 100 msec voltage commands from a holding potential of −90 mV before (Control), during 100 μM quinidine (Quinidine), and after washout of quinidine (Recovery). The voltage command paradigm is illustrated above the control current traces. (*A*2) *IV* plot of the steady state membrane current measured at the end of each voltage command for the control (circles) and quinidine (squares) data in *A*1. (*B*1) Tail currents measured from the same cell as in *A* before (Control), during 100 μM quinidine (Quinidine), and after washout of quinidine (Recovery). Tail currents were measured as described in Fig. 4, the voltage paradigm is illustrated above the control current traces. (*B*2) Tail current amplitudes plotted as a function of the test potential at which the tail current was measured for the control (squares) and quinidine (triangles) data from *B*1. Lines represent linear and third order regression fits to the control and quinidine inhibition data, respectively.

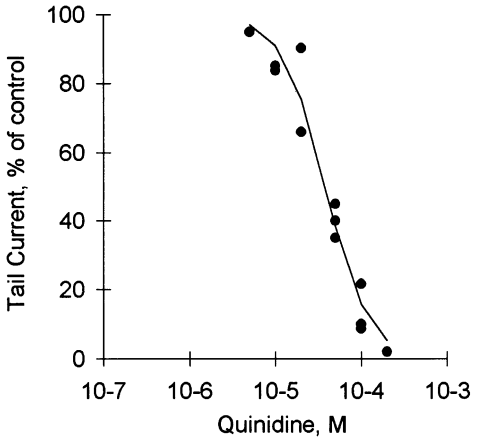

Fig. 7. Concentration dependence of quinidine-induced inhibition of tail currents. Depolarization-activated K^+ current was evoked by a voltage command to 35 mV; tail currents were measured at a test potential of −55 mV and expressed as a percentage of control. Each point represents a separate experiment. The curve represents a least squares regression fit to the Hill equation (Eq. 2).

receptor antagonist losartin but not affected by a specific AngII type 2 (AT_2) receptor antagonist [4]. Therefore if AngII-induced modulation of K^+ channels is involved in stimulation of aldosterone secretion then losartin should also inhibit AngII-induced K^+ channel modulation. In the experiment shown in Fig. 8, 0.5 μM losartin substantially blocked AngII-induced inhibition of both the leak and depolarization-activated components of K^+ current. Subsequent stimulation of the same cell with 0.5 nM AngII following washout of the preceding losartin plus AngII treatment resulted in the typical pattern of AngII-induced membrane current inhibition, demonstrating the cell was responsive to AngII. In three other experiments, pretreatment with losartin was observed to block subsequent AngII-induced inhibition of treatment current.

Characterization of Leak K^+ Channels

Spontaneously active putative single K^+ channel currents were routinely observed in cell-attached patch-clamp recordings at the resting membrane potential. However, a second channel class attributable to nonselective cation channels was also frequently observed [11]. To avoid mistaking nonselective cation channel currents for K^+ channels the ionic composition of the pipette solution was adjusted to contain a mixture of Na^+ and K^+ such that the reversal potential of K^+ selective channels differed substantially from that of nonselective cation channels.

The predominant class of putative single K^+ channel currents observed is shown in Fig. 9*A*. In this cell-attached patch the resting membrane potential was set to zero mV using high K^+ saline; the pipette contained 20 mM K^+, allowing measurable inward currents and an expected K^+ equilibrium potential of −50 mV, assuming a cytosolic K^+ concentration of 145 mM. The *IV* curve (Fig. 9*B*) plots the mean (±SEM) unitary current amplitude from seven patches measured under these conditions. The slope conductance was asymmetric due to the unequal K^+ distribution across the patch membrane; the slope conductances for the inward and outward currents were 7.8 and 12.2 pS, respectively. The average (±SD) reversal potential of the single channel currents estimated from second order regression fit of the data from each patch was −51 ± 3.4 mV.

This putative K^+ channel class characteristically exhibited a brief mean open time and low open probability (Fig. 10). The all-points current amplitude histogram of the current records shown in Fig. 9 indicated that a single channel class was present in the patch (Fig. 10*A*). The open-time histograms of unitary current events were well fit by single exponential functions (Fig. 10*B*) exhibiting time constants between 1.4 to 2.7 msec over a wide range of membrane potentials (Fig. 10*C*). The mean open times exhibited a tendency to increase with membrane depolarization but this effect was not observed in all patches. The open probability (NP_o) exhibited a biphasic response to membrane potential (Fig. 10*D*, see also Fig. 13*A*), increasing gradually in response to membrane depolarization to approximately 0 mV and much more steeply at membrane potentials above 0 mV. This patch was estimated to contain three active channels based on the maximum number of simultaneously open channels observed.

K^+ selectivity of the channel was demonstrated by the effect of the pipette K^+ concentration on the reversal potential of unitary currents recorded from cell-attached patches (Fig. 11). The slope of the linear regression fit to the data was 53.6 mV/10-fold increase in extracellular K^+ concentration.

Single-channel currents were recorded in the inside-out patch configuration and single-channel properties were similar to those obtained in cell-attached patches. However channel gating usually ran down over several minutes (approximately 5 min) in this configuration. Channel gating persisted in inside-out patches when Ca^{++} concentration was buffered to below 10^{-9} M with 5 mM EGTA on the cytosolic face indicating that channel gating was not Ca^{++}-dependent.

Contribution of Weakly Voltage-dependent K^+ Channels to Macroscopic K^+ Current

The response of weakly voltage-dependent K^+ channels to depolarization is shown in Fig. 12. Single-channel mean open times and conductance were similar to that

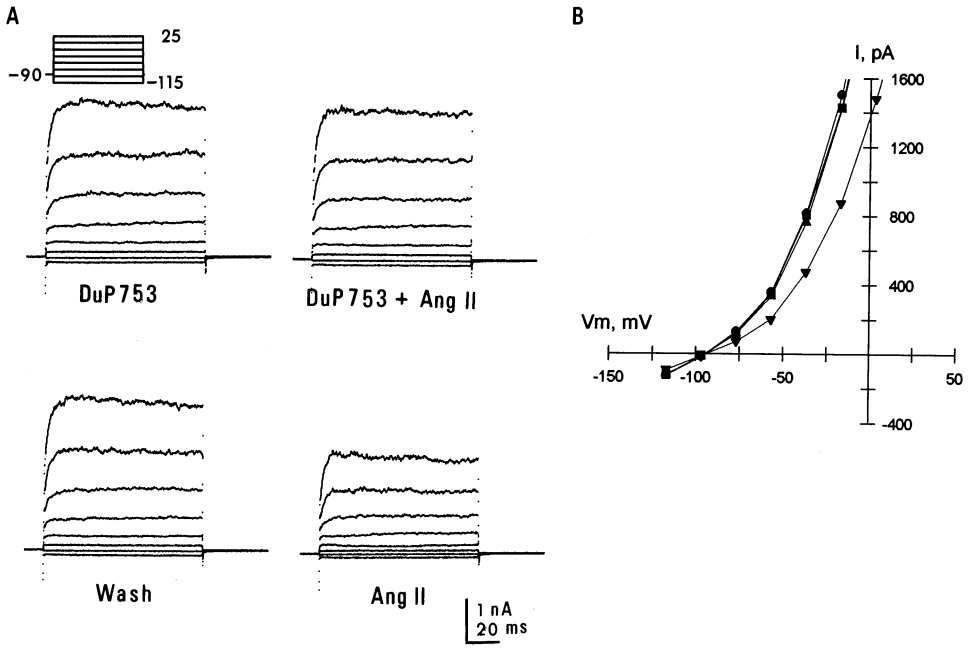

Fig. 8. The effect of losartin (DuP753) on AngII-induced inhibition of membrane current. (*A*) Superimposed current responses to 100 msec voltage commands between −115 and 25 mV in 20 mV increments in the presence of 0.5 μM losartin (DuP753), after 6 min bath stimulation with 0.5 nM AngII in the presence of 0.5 μM losartin (DuP753 + Ang II), following washout of AngII and losartin (Wash), and after 4 min bath stimulation with 0.5 nM AngII (Ang II). (*B*) *IV* relationships for the data in *A* using the current measured at the end of each voltage command for DuP753 alone (circles), DuP753 + AngII (squares), wash (triangles) and for AngII alone (inverted triangles).

described in Figs. 9 and 10 (*data not shown*). Depolarizing voltage commands rapidly evoked a stable increase in channel open probability that was maintained for the duration of the voltage command. The ensemble average of repeated patch membrane current responses indicated that these K^+ channels would produce a rapidly activating, noninactivating macroscopic current response to depolarizing voltage commands.

The proportion of the depolarization-activated macroscopic K^+ conductance represented by this K^+ channel class was estimated from the unitary channel conductance and open probability:

$$G_K = N\gamma P_o \tag{3}$$

where G_K represented the macroscopic K^+ conductance, N the number of channels available, γ the single-channel conductance, and P_o the single-channel open probability. The voltage-dependence of the single-channel open probability was estimated from nine patches with various pipette K^+ concentrations so that single-channel events could be clearly measured over a wide range of membrane potentials (Fig. 13*A*). Saturation of the open probability was not observed in these experiments as most patches became unstable at potentials above 50 mV. The smooth curve represents the fit of these data to a Boltzman equation of the form:

$$P_o = P_{max}/[1 + \exp((V_{0.5} - V_m)/k)] \tag{4}$$

where P_{max} is the maximum single channel open probability, V_m the membrane potential, $V_{0.5}$ the membrane potential at which P_o is one half maximum, and k the slope factor. The fit predicted a P_{max} of 0.27, $V_{0.5}$ of 81.9 mV, and the slope factor of 74.5 mV.

Macroscopic steady state K^+ conductance calculated from nystatin perforated-patch clamp measurement of membrane current is shown in Fig. 13*B;* membrane current records were not leak subtracted. K^+ conductance was calculated as a chord conductance from the membrane current at the end of 100 mS voltage clamp pulses and assuming a K^+ equilibrium potential of −85 mV and steady state membrane current entirely due to K^+. These data represent the average of 13 cells which ranged in membrane capacitance between 4 and 20 pF. K^+ conductance was not observed to saturate even at membrane potentials up to 100 mV (*data not shown*).

The macroscopic K^+ conductance that could be maximally attributed to the weakly voltage-dependent K^+ channel was calculated using Eq. 3 and is indicated by dotted line in Fig. 13*B.* This calculation suggested that this channel class may account for most but not all of the K^+ conductance at membrane potentials below 0 mV. Deviation of the curves at membrane potentials below −80 mV may be attributed to ohmic leakage currents

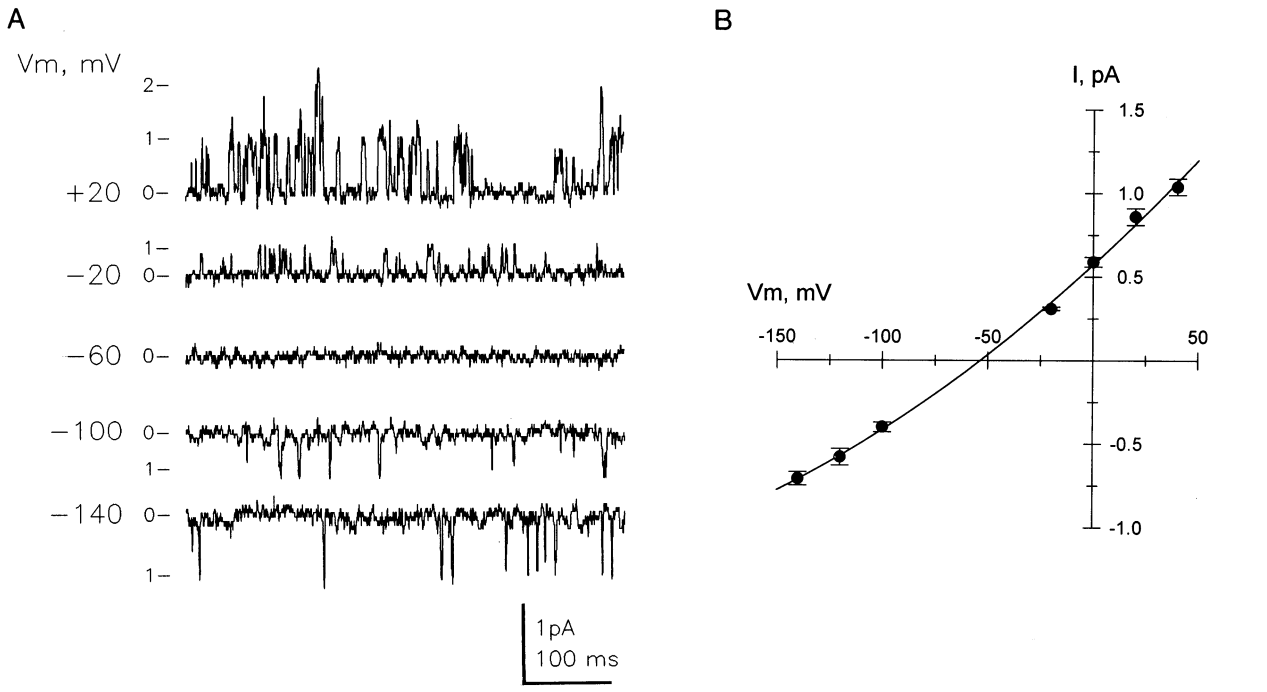

Fig. 9. Cell-attached patch clamp recording of single K^+ channel currents. (*A*) Representative examples of steady-state single-channel activity (20 mM K^+ pipette solution) measured at several patch membrane potentials (indicated at left of each current trace). The current level corresponding to 0, 1 or 2 simultaneously open channels is indicated at the left of each trace. The cell resting membrane potential was set to zero with a high K^+ bath saline. Current records were digitally filtered at 500 Hz for display. (*B*) Mean (±SEM) of unitary current amplitude from seven patches plotted as function of patch membrane potential. The curve represents a second order regression fit to the data.

not subtracted from the macroscopic current records. The average number of K^+ channels in 1 pF of membrane was estimated from the macroscopic G_K at −60 mV to be approximately 870, assuming an outward single-channel conductance of 10 pS in 4 mM extracellular K^+ (*data not shown*) and that these channels accounted for all the K^+ conductance at this potential. This calculation further assumed an estimated inward single-channel conductance of 4.5 pS in 4 mM extracellular K^+ and utilized the voltage-dependent open probability described by the Boltzman equation fit of the single-channel open probability from Fig. 13*A*.

These calculations suggest that at least one other class of voltage-dependent K^+ channel contributed to macroscopic K^+ conductance. In agreement with these calculations, inclusion of 100 μM quinidine in the pipette saline of single-channel recordings only partially inhibited the weakly voltage-dependent K^+ channel, reducing the mean open time and NP_o but not significantly affecting single channel current amplitude (*data not shown*). These effects were consistent with an open channel blocking mechanism for quinidine [22].

AngII Modulation of Leak K^+ Channel

Bath stimulation with AngII reversibly inhibited opening of the weakly voltage-dependent K^+ channels in cell-attached patches (Fig. 14). In the experiment shown the pipette solution contained 145 mM/L K^+, allowing measurement of single channel currents despite AngII-induced membrane depolarization; the cell membrane potential was not controlled in these experiments. At this pipette K^+ concentration channels exhibited an inward single channel conductance of 24 pS based on the slope conductance of the mean unitary currents and were identified based on their apparent reversal potential (extrapolated from an expected resting membrane potential of −85 mV), a voltage-independent mean open time of approximately 2.0 msec, and a low single channel open probability. Bath stimulation with AngII reversibly decreased NP_o over the entire range of potentials examined (Fig. 14*B*) indicating that observed changes in single channel current were not attributable to AngII-induced changes in cell membrane potential. Reversal of AngII inhibition of NP_o required approximately 20 min after washout of AngII.

Discussion

In the present study we observed two patterns of macroscopic *IV* relationships in cultured rat glomerulosa cells similar to those reported previously for rat cells [3,

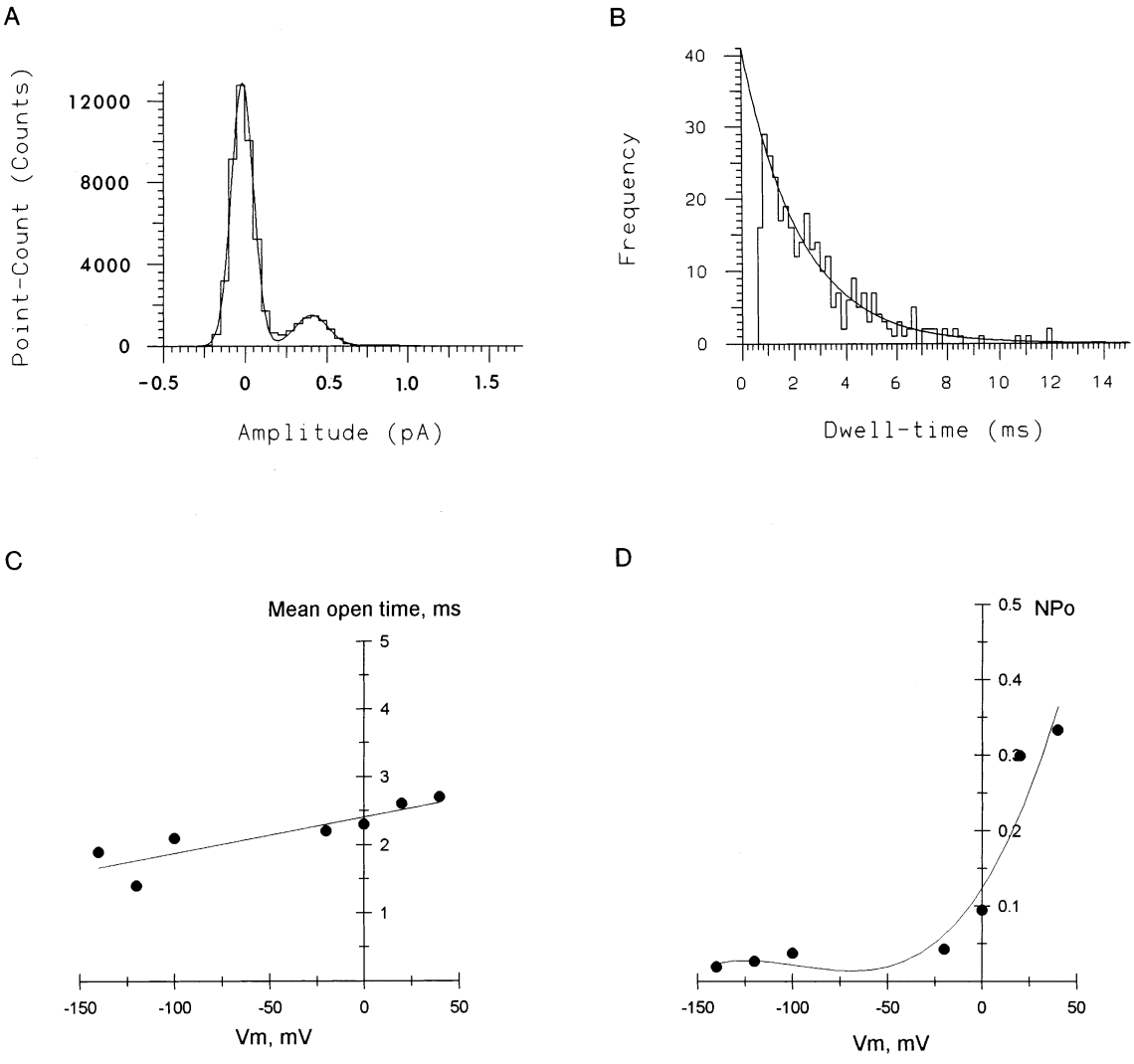

Fig. 10. Mean open time and open probability of single channel events from the cell-attached patch current records shown in Fig. 9*A*. (*A*) All-points current amplitude histogram of the current record at a patch membrane potential of 0 mV. The smooth curve represents two Gaussian distributions corresponding to current levels of the closed and open states; a third peak corresponding to two open channels is not observable at this scale. (*B*) Open state dwell time histogram of single channel events at a patch membrane potential of 0 mV. The curve represents a single exponential fit exhibiting a time constant of 2.3 mS. (*C*) Mean open times determined from single exponential fits to open state dwell time histograms plotted as a function of the patch membrane potential. The curve represents a linear regression fit to the data. (*D*) NP_o, calculated as described in methods, plotted as a function of patch membrane potential. The patch was estimated to contain three active channels based on the maximum number of simultaneously open channels observed. The curve represents a third order regression fit to the data.

17]. The type 1 *IV* pattern was characterized by a weakly voltage-dependent component of K^+ current active at the resting membrane potential and a rapidly activating, noninactivating voltage-dependent component apparent in response to membrane depolarizations above −50 mV. The type 1 pattern occurred in the majority of cells recorded after 12 hr in culture and was observed in the few acutely dissociated cells examined, suggesting that this may represent the predominant phenotype *in vivo.* In contrast to previous whole-cell recordings of macroscopic current in ''type 1'' glomerulosa cells [3], we were able to measure AngII inhibition of a macroscopic K^+ current active at the resting membrane potential. Furthermore, treatments that inhibited Ca^{++} influx (lowering extracellular Ca^{++} concentration, organic and inorganic Ca^{++} channel blockers) did not significantly affect membrane current, indicating that type 1 cell K^+ channels were not Ca^{++}-dependent. The type 2 pattern was characterized by a transient depolarization-activated outward K^+ current mediated by charybdotoxin-sensitive Ca^{++}-dependent K^+ channels. The observation that the type 2 pattern was more common in older cultures might sug-

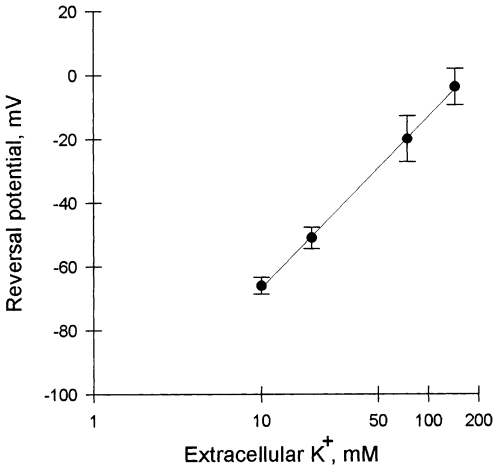

Fig. 11. The reversal potential of unitary currents measured over a range of extracellular (pipette) K^+ concentrations in cell-attached patches with resting membrane potential set to 0 mV with high K^+ saline. Symbols indicate the mean ± SD of the reversal potentials; sample sizes were 3, 7, 4 and 6 for 10, 20, 75 and 145 mM K^+ pipette solutions, respectively. The curve represents a linear regression fit to the data.

gest that this *IV* pattern was induced during cell culture. Ca^{++}-dependent K^+ channels also predominate the depolarization-activated outward current of clonal adrenocortical Y1 cells [23].

K^+ Channel Classes in the Type 1 Cells

The present study identified only one class of K^+ channel at the single-channel level, a weakly voltage-dependent channel that was spontaneously active at the resting membrane potential. This channel predominated in membrane patches such that it was difficult to obtain membrane patches that did not contain multiple active channels of this class. The outwardly rectifying conductance properties (due to asymmetric K^+ distribution across the membrane) and weakly voltage-dependent gating properties of this channel are predicted to generate a macroscopic current that closely matches the characteristics of the measured macroscopic K^+ current at membrane potentials below approximately −40 mV. These observations suggest that this channel class dominated the macroscopic K^+ current at membrane potentials below −40 mV. The tendency for channel gating to run-down in inside-out patches may offer an explanation for the failure of previous whole-cell patch clamp experiments to observe AngII inhibition of macroscopic current at more negative membrane potentials [3, 16].

Previous cell-attached patch clamp studies on acutely dissociated rat glomerulosa cells reported an inwardly rectifying 42 pS K^+ channel to be the predominant K^+ channel active at the resting membrane potential

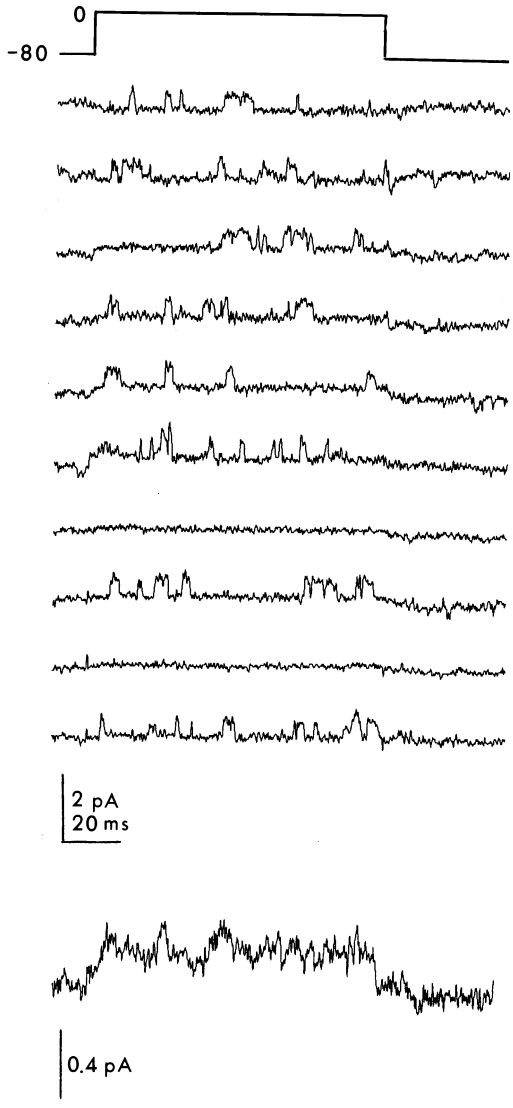

Fig. 12. Single K^+ channel gating responses in a cell-attached patch to repeated 100 mS depolarizing voltage commands from a holding potential of −80 to 0 mV. The top trace illustrates the time course of the voltage command; subsequent traces illustrate consecutive single channel current response to the voltage pulse. The bottom current trace represents the ensemble average of twenty-five patch current responses to the voltage pulse. The resting membrane potential was set to 0 mV with high K^+ saline. Capacitive transients and leak were subtracted; displayed current traces and the ensemble average were digitally filtered at 1,000 Hz for display.

[24]. Control of the resting membrane potential by an inward rectifier, as opposed to the weakly voltage-dependent K^+ channel described in the present study, would have important consequences for membrane potential responses to activation of inward current, increasing the magnitude and duration of depolarization and consequently affecting patterns of Ca^{++} influx. However, no evidence of an inwardly rectifying macroscopic K^+ current in the type 1 cells was observed in the present

study or in previous whole-cell patch clamp studies [3]. The 42 pS inwardly rectifying channel described by Vassilev et al. [24] differed substantially from the K^+ channel described in the present study. Under similar recording conditions (145 mM K^+ pipette solution), the weakly voltage-dependent channels exhibited an inward single-channel conductance of 24 pS, a mean open time of 2 mS, and a low open probability as opposed to a 42 pS conductance, a mean open time of 0.38 mS and a high open probability (0.15 at −80 mV) for the inwardly rectifying channel [24]. It would appear possible that the inward rectifier described by these authors represented inwardly rectifying nonselective cation channels reported in rat adrenal glomerulosa cells [11]. Otherwise we must hypothesize the unlikely possibility that all of our patches contained two classes of K^+-selective channels of similar conductance and gating properties such that an outwardly rectifying channel masked the inwardly rectifying property of the channel mediating inward currents.

Depolarization-activated K^+ Current

Several indirect lines of evidence suggested that a second class of depolarization-activated, noninactivating K^+ channel contributed to macroscopic K^+ currents at membrane potentials above −50 mV. Depolarization-activated outward current usually recovered from AngII inhibition more rapidly than leak current. The steady state outward slope conductance of Cs^+-loaded cells increased nearly threefold at positive membrane potentials relative to negative membrane potentials. Quinidine appeared to selectively inhibit a depolarization-activated component of membrane current. Finally, the predicted macroscopic current attributable to the weakly voltage-dependent K^+ channel was insufficient to account for the increase in macroscopic K^+ conductance at membrane potentials above −40 mV. These observations may also have other explanations.

A strongly voltage-dependent K^+ channel class with properties consistent with the macroscopic current has not yet been characterized in rat glomerulosa cells. Identification of a second class of strongly voltage-dependent K^+ channel may require selective pharmacological blockers to reduce interference from the weakly voltage-dependent K^+ channels. Strongly voltage-dependent apparent single K^+ channel currents exhibiting a larger single channel conductance and long open times were observed in some cell-attached and inside-out patches. However, such channels have not been observed often enough in the absence of multiple weakly voltage-dependent K^+ channels to characterize their ion selectivity and gating properties. Previous cell-attached patch clamp studies described two K^+ permeable channels hypothesized to mediate delayed rectification in rat glomerulosa cells [24]. These channels were reported to exhibit single channel conductances of 48 pS and 27 pS (150 mM K^+ pipette solution) and were reported to be active at the resting membrane potential. The more thoroughly characterized 27 pS channel was more commonly observed (40% of patches) and was also reported to be

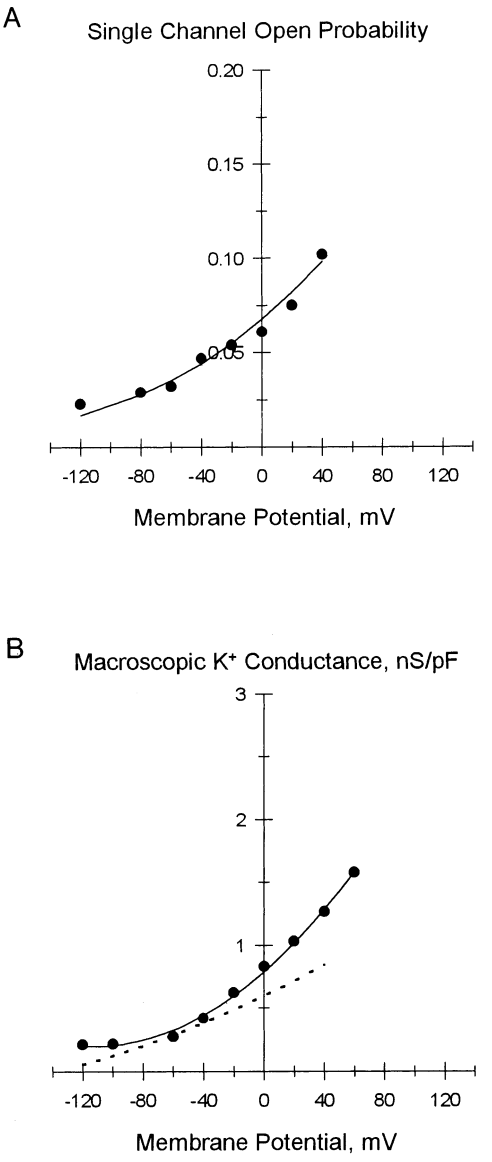

Fig. 13. Modeling of the maximum macroscopic K^+ conductance that may be attributed to the weakly voltage-dependent K^+ channel. (*A*) Voltage-dependence of the mean single channel open probability determined from nine patches. The curve represents the fit of the data to a Boltzman distribution (Eq. 4). (*B*) Voltage-dependence of mean macroscopic K^+ conductance measured from 13 cells using nystatin perforated-patch clamp current measurements (*see text for explanation*). The smooth curve represents a second order regression fit to the data. The dotted line represents the maximum macroscopic K^+ conductance attributable to the weakly voltage-dependent K^+ channel, assuming 870 channels per pF (*see text for explanation*).

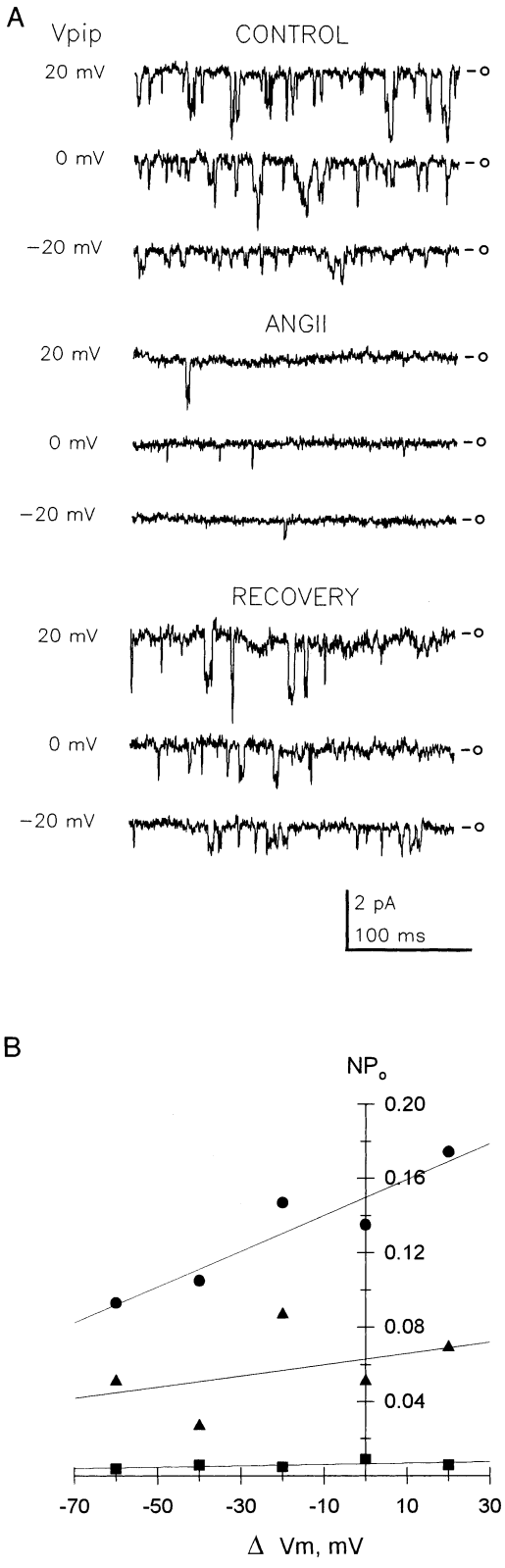

Fig. 14. Effect of bath stimulation with AngII on spontaneously active K^+ channels in a cell-attached patch. (*A*) Current traces illustrate representative steady state channel gating activity before (Control), 3 min after onset of bath stimulation with 1.0 nM AngII (AngII), and 15 min after washout of AngII (Recovery). The patch membrane potential was equal to the cell membrane potential minus the pipette command potential (Vpip). (*B*) The open probability plotted as a function of changes in patch membrane potential produced by pipette polarization for the control (circles), AngII (squares) and recovery (triangles) data. The patch contained at least three active channels in the control condition. Curves represent linear regression fits to the data.

inhibited by AngII [10]. The open probability of the 27 pS channel was reported to increase from 0.28 at a membrane potential of −50 to 0.42 at 50 mV. This relatively small change in open probability would appear unlikely to account for the increase in macroscopic K^+ conductance occurring over this range of membrane potentials.

In summary, AngII-induced effects on glomerulosa cell plasma membrane ion conductances will dictate membrane potential changes and patterns of Ca^{++} influx. Consequently, AngII-regulated ion channels represent an important component of the signal transduction processes controlling aldosterone secretion. Regulation of K^+ channels is expected to be an important component of membrane depolarization. AngII control of K^+ conductances was found to be mediated through activation of the AT_1 receptor which was previously shown to mediate AngII-induced aldosterone secretion [4] and is consistent with previous reports that losartin inhibited AngII-induced inhibition of ^{86}Rb flux [6], Ca^{++}-dependent maxi-K^+ channels [16], and elevation of cytosolic Ca^{++} concentration [1]. The properties of the weakly voltage-dependent K^+ channel suggested that this channel functions to maintain the resting membrane potential and AngII inhibition of this channel class will have an important role in initiating membrane depolarization. However, AngII modulation of other channel classes, such as nonselective cation channels [11], may also contribute to AngII-induced membrane depolarization and stimulation of Ca^{++} influx in adrenal glomerulosa cells. AngII inhibition of other depolarization-activated K^+ channels is hypothesized to increase the amplitude and duration of membrane depolarizations initiated by activation of inward currents, allowing recruitment of high threshold, voltage-dependent Ca^{++} channels.

This work was supported by Grants-in-aid from the American Heart Association, Illinois Affiliate and Kentucky Affiliate.

References

1. Ambroz, C., Catt, K.J. 1992. Angiotensin II receptor-mediated calcium influx in bovine adrenal glomerulosa cells. *Endocrinology* **131:**408–414
2. Barrett, P.Q., Bollag, W.B., Isales, C.M., McCarthy, R.T., Rasmussen, H. 1989. Role of calcium in angiotensin II-mediated aldosterone secretion. *Endocrine Reviews* **10:**496–518
3. Brauneis, U., Vassilev, P.M., Quinn, S.J., Williams, G.H., Tillotson, D.L. 1991. ANG II blocks potassium currents in zona glomerulosa cells from rat, bovine, and human adrenals. *Am. J. Physiol.* **260:**E772–E779

4. Chang, R.S., Lotti, V.J. 1990. Two distinct angiotensin II receptor binding sites in rat adrenal revealed by new selective nonpeptide ligands. *Mol. Pharmacol.* **37:**347–351
5. Finkelstein, A. 1987. Water Movement through Lipid Bilayers, Pores, and Plasma Membranes: Theory and Reality. Vol. 4, p. 127. Wiley-Interscience, New York
6. Hajnoczky, G., Csordas, G., Bago, A., Chiu, A.T., Spat, A. 1992. Angiotensin II exerts its effect on aldosterone production and potassium permeability through receptor subtype AT_1 in rat adrenal glomerulosa cells. *Biochem. Pharmacol.* **43:**1009–1012
7. Hamill, O.P., Marty, A., Neher, E., Sakmann, B., Sigworth, F.J. 1981. Improved patch-clamp techniques for high-resolution current recording from cells and cell-free membrane patches. *Pfluegers Arch.* **391:**85–100
8. Horn, R., Marty, A. 1988. Muscarinic activation of ionic currents measured by a new whole-cell recording method. *J. Gen. Physiol.* **92:**145–159
9. Hornsby, P.J., McAlister, J.M. 1991. Culturing steroidogenic cells. *Methods Enzymol.* **206:**371–380
10. Kanazirska, M.V., Vassilev, P.M., Quinn, S.J., Tillotson, D.L., Williams, G.H. 1992. Single K^+ channels in adrenal zona glomerulosa cells II. Inhibition by angiotensin II. *Am. J. Physiol.* **263:**E760–E765
11. Lotshaw, D.P., Li, F. 1996. Angiotensin II activation of Ca^{++}-permeant nonselective cation channels in rat adrenal glomerulosa cells. *Am. J. Physiol.* **271**:C1705–C1715
12. Matsunaga, A., Maruyama, Y., Kojima, I., Hoshi, T. 1987. Transient Ca^{++} channel current characterized by a low threshold voltage in zona glomerulosa cells of rat adrenal cortex. *Pfluegers Arch.* **408:**351–355
13. McCarthy, R.T., Isales, C.M., Bollag, W.B., Rasmussen, H., Barrett, P.Q. 1990. Atrial natriuretic peptide differentially modulates T- and L-type calcium channels. *Am. J. Physiol.* **258:**F474–F478
14. Neher, E. 1992. Correction for liquid junction potentials in patch clamp experiments. *Methods Enzymol.* **207:**123–131
15. Payet, M.D., Benabderrazik, M., Gallo-Payet, N. 1987. Excitation-secretion coupling: ionic currents in glomerulosa cells: effects of adrenocorticotropin and K^+ channel blockers. *Endocrinology* **121:**875–882
16. Payet, M.D., Bilodeau, L., Drolet, P, Ibarrondo, G.G., Gallo-Payet, N. 1995. Modulation of a Ca^{2+}-activated K^+ channel by angiotensin II in rat adrenal glomerulosa cells: involvement of a G protein. *Mol. Endocrinol.* **9:**935–947
17. Payet, M.D., Durroux, T., Bilodeau, L., Guillon, G., Gallo-Payet, N. 1994. Characterization of K^+ and Ca^{2+} ionic currents in glomerulosa cells from human adrenal glands. *Endocrinology* **134:**2589–2598
18. Quinn, S.J., Cornwall, M.C., Williams, G.H. 1987. Electrical properties of isolated rat adrenal glomerulosa and fasciculata cells. *Endocrinology* **120:**903–914
19. Quinn, S.J., Cornwall, M.C., Williams, G.H. 1987. Electrophysiological responses to angiotensin II of isolated rat adrenal glomerulosa cells. *Endocrinology* **120:**1581–1589
20. Roskelley, C.D., Auersperg, N. 1990. Density separation of rat adrenocortical cells: morphology, steroidogenesis, and P-450scc expression in primary culture. *In Vitro Cell. Dev. Biol.* **25:**493–501
21. Spat, A. 1988. Stimulus-secretion coupling in angiotensin-stimulated adrenal glomerulosa cells. *J. Steroid Biochem.* **29:**443–453
22. Synders, D.J., Knoth, K.M., Roberds, S.L., Tamkun, M.M. 1992. Time-, voltage-, and state-dependent block by quinidine of a cloned human cardiac potassium channel. *Molec. Pharmacol.* **41:**322–330
23. Tabares, L., Urena, J., Lopez-Barneo, J. 1989. Properties of calcium and potassium currents of clonal adrenocortical cells. *J. Gen. Physiol.* **93:**495–519
24. Vassilev, P.M., Kanazirska, M.V., Quinn, S.J., Tillotson, D.L., Williams, G.H. 1992. K^+ channels in adrenal zona glomerulosa cells I. Characterization of distinct channel types. *Am. J. Physiol.* **263:**E752–E759